SCIENCE CHINA
Technological Sciences

• Article •

February 2018 Vol.61 No.2: 309–316
https://doi.org/10.1007/s11431-017-9149-1

The effect of surface anisotropy on contact angles and the characterization of elliptical cap droplets

WANG ZhanLong[1,2], CHEN EnHui[1,2] & ZHAO YaPu[1,2*]

[1] *State Key Laboratory of Nonlinear Mechanics, Institute of Mechanics, Chinese Academy of Sciences, Beijing 100190, China;*
[2] *School of Engineering Science, University of Chinese Academy of Sciences, Beijing 100049, China*

Received July 28, 2017; accepted September 12, 2017; published online October 23, 2017

In this paper, the variation of contact angles of a droplet on grooved surfaces was studied from microscale to macroscale experimentally and theoretically. The experimental results indicated that the contact angle changes nonlinearly with anisotropic factor. To get clear of the changing process of contact angle on grooved surfaces from microscale to macroscale, we carried out theoretical analysis with moment equilibrium method being adopted. In addition, the variation of contact angles in different directions was investigated and a mathematic model to calculate arbitrary contact angles around the elliptic contact line was suggested. For the convenience of potential applications, a symbolic contact angle was proposed to characterize the ellipsoidal cap droplet on grooved surfaces. Our results will offer help to the future design of patterned surfaces in practical applications, and deepen the understanding of wetting behavior on grooved surfaces.

droplet, contact angle, ellipse, contact line, grooved surface

Citation: Wang Z L, Chen E H, Zhao Y P. The effect of surface anisotropy on contact angles and the characterization of elliptical cap droplets. Sci China Tech Sci, 2018, 61: 309–316, https://doi.org/10.1007/s11431-017-9149-1

1 Introduction

Wetting on solid surface is ubiquitous in nature [1–9], and is of key importance in a wide range of industrial applications, such as bionics [10,11], materials test [12,13], microfluidics [4], super-hydrophobic materials [14] and microchips [6]. In recent years, wetting on grooved surface (GS) has attracted increasing scientific and technological attention [15–19]. This is mainly driven by the rapid development in the applications of GS in self-clean surface [20], directional transport [6,21–23], fog-harvesting [7,24] and so on. Compared with spherical shapes of droplets on isotropic surfaces, droplets exhibit long strip shapes [25] or ellipsoidal shapes on GS, and thus the droplets have different apparent contact angles (CAs) in different directions, as shown in Figure 1. The surface structure usually has significant influence on the apparent CAs. However, a systemic study from microscale to macroscale on droplet CAs on GS is rare. Until now, there are no simple yet effective methods to characterize a droplet on GS for the convenience of related wetting experiments and industrial products. For further utilization of the GS in potential applications, it is essential to understand fundamental issues, including the variation of CA with anisotropic surface morphology and the characterization of droplet properties on GS.

When a droplet is deposited on an isotropic rough surface, CA is described by Wenzel [26] or Cassie-Baxter equation [27]. The Wenzel equation is:

$$\cos\theta_c = r_o \cos\theta_0, \tag{1}$$

and the Cassie-Baxter equation is:

$$\cos\theta_c = r_1 \cos\theta_0 - r_2, \tag{2}$$

Corresponding author (email: yzhao@imech.ac.cn)

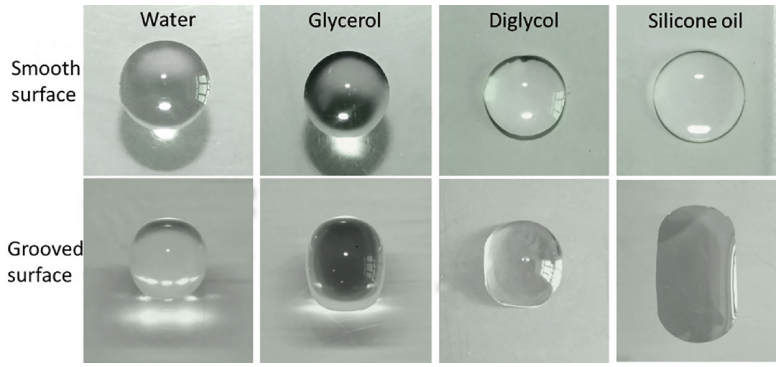

Figure 1 Droplet shapes of different liquids on smooth surfaces and GSs. The surface tensions of them in the order decrease. These droplets exhibit spherical caps on smooth surfaces and elongated shapes on GS. Water, glycerol and diglycol droplets show ellipsoidal cap shapes, and silicone oil droplet shows a long strip shape on GS.

where *ro* is the surface roughness, defined as the ratio of the actually wetted area to the projected area under droplet. r_1 and r_2 are the fractions of the surface area occupied by water and air. θ_c and θ_0 are CAs on rough surface and homogeneous smooth surface, respectively. This formulation describes the effect of surface roughness on CA. However, a droplet placed on GS is affected by not only the surface roughness, but also the difference of geography in two different directions. As a result, the CAs in different directions are different and the shape of droplet is no longer spherical. There is obvious deficiency for the CA determination with Wenzel or Cassie-Baxter equation. On GS, a droplet will be elongated along grooves and be compressed in perpendicular direction. This is because of the absence of contact line pinning in parallel direction and obvious contact line pinning in perpendicular direction. When the surface structure changes, the shape of droplet changes accordingly. So, having a clear understanding of how the surface structure affects CAs and how the CAs vary in different directions becomes significant. Previous works reported that the CA in the direction parallel to the grooves was close to CA on flat surface in microscale [28–32]. Kusumaatmaja et al. [33] pointed out that the CA in parallel direction obeys Wenzel equation approximately in a plenty of experiments. Chung et al. [34] also reported that CA in the direction parallel to grooves follows Wenzel equation on corrugated surfaces. Despite of numerous reports on CA in parallel direction, the study on CA in perpendicular direction is relatively less. Moreover, until now, the existing theories are not recognized generally. A systematic study on CA on GS from microscale to macroscale is needed. And the liquid filaments and precursor film [35,36] that may occur in grooves also deserve a further study.

The discrepant CAs in different directions on GS bring inconvenience in the characterization of wetting properties. A uniform and effective method will be helpful. In the past, two CAs of θ_x and θ_y were usually adopted to describe the droplet on GS [37], where θ_x and θ_y are CAs observed from perpendicular and parallel directions, respectively. However, it is inconvenient in lots of aspects, e.g., the definitions of hydrophobicity or hydrophilicity of GS, the related wetting experiments in medicine, electronics and so on. Fractal theory was ever adopted to describe the relationship between CA and surface morphology [38]. However, this theory lacks convenience in real systems and does not consider the anisotropy of surface structure.

In this paper, we measured CAs of droplets on GS from microscale to macroscale experimentally, and gave a theoretical analysis between CA and anisotropic roughness with moment equilibrium method. Furthermore, we provided a mathematic method to get an arbitrary CA in the elliptic contact line. A simple yet effective method was provided to characterize the wettability of droplet on GS. Our results may offer help to the industrial designs and potential engineering applications in the future, and deepen the understanding of wetting on GS.

2 Materials and methods

We first fabricated grooved substrates with SU-8 photoresist using standard photolithographic method. Then the samples were used as molds for patterning polydimethylsiloxane (PDMS, Sylgard 184, Dow Corning, USA) substrates [34]. The substrates used in the experiments were prepared in the following way: (1) curing with the mass ratio of the base to coupler of 10:1; (2) PDMS was spin-coated on the molds at 800 r/min for 40 s; (3) baking the substrates at 150°C for 20 min; (4) peeling the PDMS films off from molds. After these processes, PDMS samples with grooves were ready for experiments. For these samples, the depth d of the groove is fixed, 35 μm. The groove width w_1 and the ridge width w_2 (as illustrated in Figure 2) range from 10 μm to 500 μm. The groove period $D = w_1 + w_2$.

Droplets of deionized (DI) water and glycerol with volumes ~4 μL were used in experiments. The droplet shapes were observed from top view and CAs were measured from side view and front view, respectively. X and Y represent the directions of side view and front view, respectively, as shown in Figure 2. The droplet shapes and CAs were captured using a high-magnification microscope (KH-8700, Hirox, USA) and

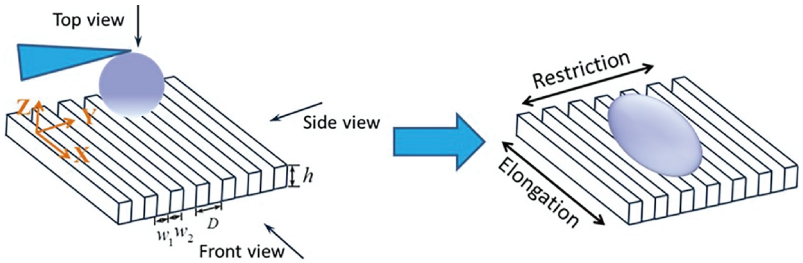

Figure 2 (Color online) A sessile droplet deposited on GS. Our observations include top view, side view and front view. The X and Y are defined as the directions observed from side view and front view, respectively. w_1, w_2, h and D are the groove width, ridge width, groove depth and groove period, respectively.

contact angle measurement system (OCA20, Data physics, Germany), respectively, as shown in Figure 3.

We mainly studied the influence of roughness in X and Y directions on droplets. A parameter $S_c = ro_y / ro_x$ was introduced, donoting the ratio of the roughness between X and Y directions. ro_x, ro_y are the roughness in X and Y directions, respectively, where $ro_x = (w_1 + w_2 + 2h)/(w_1 + w_2)$, $ro_y = 1$ for GS. The values of S_c of different samples are shown in Table 1. The groove depth of sample is fixed, while the widths of groove and ridge are varied.

3 Results and discussion

3.1 The relationship between CA and anisotropic roughness on GS

To understand the mechanism that how the anisotropic roughness affects CA on GS from microscale to macroscale, we carried out experiments and theoretic analysis. The experimental results are shown in Figure 4. The vertical coordinate represents the ratio of θ_c to θ, where θ_c is CA on GS, and θ is CA on smooth surface. The horizontal coordinate represents the roughness ratio of Y to X direction. From experimental results, we found that CAs of a droplet on GS are larger than that on flat surfaces the anisotropic rough morphology. CAs in X direction are larger than that in Y direction, and this is in agreement with previous reports [22,25,28]. In microscale, CAs change with surface morphology in a monotonous relation [37]. However, CAs follow a nonlinear relation when the surface structure changes from microscale to macroscale.

Table 1 Substrates with different anisotropic roughness used in the experiments

Sample	w_1 (μm)	w_2 (μm)	S_c
1	8	8	0.21
2	16	16	0.32
3	10	25	0.4
4	24	24	0.57
5	32	32	0.68
6	64	64	0.83
7	128	128	0.91
8	256	256	0.98

The CAs of DI water droplets on GS are shown in Figure 4(a). From the results, we found that CA increases first and then decreases with S_c in both X and Y directions. The trend of CA changing with S_c can be divided into two stages: (1) CA increases with increasing S_c. In this stage, as S_c increases, the roughness plays an increasing role on CA. The reason is that the surface with infinitesimal roughness approaches smooth surface. (2) CA decreases with increasing S_c. Since the roughness effect was weakened with the increasing groove period. When the period of surface structure becomes infinite, the CA on GS is close to that on smooth surface. Thus, there exists a critical value that distinguishes the two stages, and this value differs in X and Y directions. From the results, we found the critical values are around 0.6 and 0.45 in X and Y directions, respectively. The CAs of glycerol droplets on GS are shown in Figure 4(b), and the changing process is similar to that of DI water droplets on GS.

The snapshots of DI water droplets from X direction and the corresponding substrates are shown in Figure 5. The CAs and S_c of different substrates are: (1) θ_x=90.6°, S_c=0.21; (2) θ_x=134.6°, S_c=0.40; (3) θ_x=142.2°, S_c=0.68; (4) θ_x=91.2°, S_c=0.98, respectively. The CAs presented here follow the tendence of the variation of CA, i.e. increase first and then decrease during the process of the succession of S_c. The results agree with the descriptions in Figure 4.

The mechanism for the second stage is illustrated in Figure 6(a). For GS, S_c increases with increasing groove period. When a droplet is deposited on GS where the groove period is quite small, the contact line will be driven to step forward under the attraction between droplet and next ridge in X direction. The droplet reaches a stable state when the attractive force is balanced by Laplace pressure. Driven by this attraction, the droplet propagates in X direction until it reaches equilibrium state. As the groove period decreases, the droplet propagates in X direction further. For a droplet with fixed volume, CA decreases as wetted area increases, i.e., CA increases with increasing S_c. When the groove period decreases to a sufficiently small value, the state of a droplet on GS is similar to that on smooth surface, and the CA tends to be the value on smooth surface.

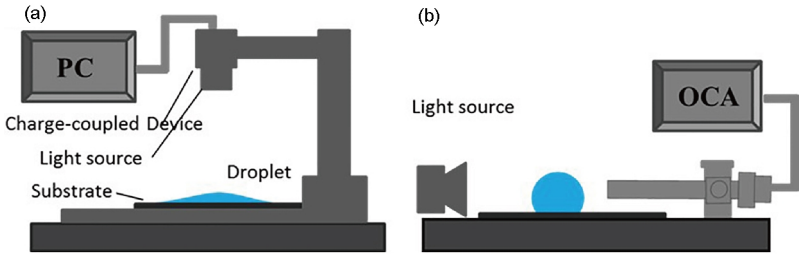

Figure 3 (Color online) The schematics of the experimental setups. (a) The observation system of high-magnification microscope; (b) the contact angle measurement system.

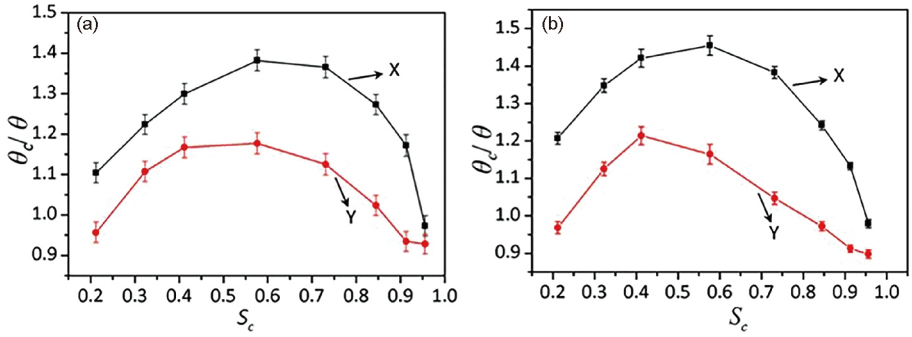

Figure 4 (Color online) CAs on GS with different S_c. The vertical coordinate represents the ratio of θ_c to θ, where θ_c and θ are CAs on GS and smooth surface, respectively. X and Y represent the CAs measured in X and Y directions, respectively. (a) CAs of DI water droplets; (b) CAs of glycerol droplets.

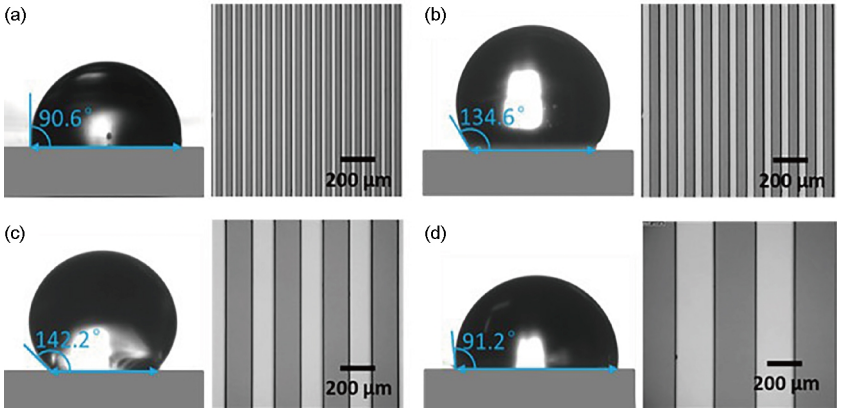

Figure 5 (Color online) The front view snapshots of droplet on varied GS, and the corresponding substrates. (a) θ_x=90.6°, S_c=0.21; (b) θ_x=134.6°, S_c=0.40; (c) θ_x=142.2°, S_c=0.68; (d) θ_x=91.2°, S_c=0.98.

Theoretical analysis was carried out to understand the underlying mechanism of the relation between CA and S_c. For rough surfaces, the equilibrium state of a droplet is determined by the balance of interfacial tensions. The equilibrium CA can be described by Wenzel or Cassie-Baxter equation. However, Wenzel or Cassie-Baxter equation needs to be modified for the description of droplets on GS, due to the contact line pinning in X direction and no pinning in Y direction. The pinning force hinders the droplet from stretch or movement, leading to the increase or decrease of CAs. How the pinning of contact line affects the change of CA? To address this problem, the equilibrium of couples is adopted. We assume that the pinning force acting in contact line conforms to the rule of equilibrium of couples, and suppose that the arm of couple of pinning force is l, the droplet surface stiffness is k, and the CA change is $\Delta\theta$. The schematic diagram is shown in Figure 6(c). These parameters follow:

$$f \cdot l = k \cdot \Delta\theta, \tag{3}$$

where the surface stiffness scales as $k \sim \lambda\gamma_{lv}$ [39,40], and λ has a dimension of length L. k has the dimension of force MLT^{-2}. $\Delta\theta$ in radian is a non-dimensional parameter, l has a dimension of length L. So f should have a dimension of force per unit length MT^{-2}.

In previous reports, the pinning force f has the expression of $f = \gamma_{lv}(\cos\theta_a - \cos\theta)$ or $f = \gamma_{lv}(\cos\theta - \cos\theta_r)$ [41], where θ_a is the advancing CA and θ_r is the receding CA. The value of pinning force changes as the boundary conditions vary.

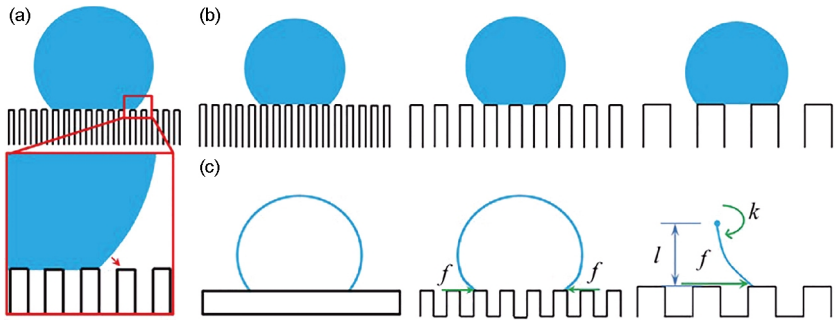

Figure 6 (Color online) Illustration of the propagation of a droplet on GS in X direction. (a) Droplet on GS. The droplet contact line will be driven to step forward under the attraction between droplet and the ridge in X direction. (b) The droplets on GS with the groove width from left to right being 5, 8, 15 μm. The semi axis of the elliptic contact line in X direction is 27.5, 20, 22 μm. The pinning force increases as the semi axis of the elliptic contact line decreases. The droplet on GS with groove width being 8 μm suffers largest pinning force compared to the other surfaces. (c) The schematic diagram of a droplet on: smooth surface; GS (the pinning force acts on the contact line in the ridge edge); the pinning force is balanced by the surface stiffness, l is the arm of couple, k is the surface stiffness of droplet.

Figure 6(c) exhibits the droplets of the same volume on GS with the groove widths being 5, 8 and 15 μm, respectively. And the semi-major axes of elliptic contact line in X direction are 27.5, 20 and 22 μm, respectively. Obviously, the droplet has a larger semi-major axis on the surface with groove width being 5 μm than 8 μm, and this is due to the attraction between droplet and ridge as depicted in Figure 6(a). The semi-major axis on surface with groove width 15 μm is larger than that with 8 μm, owing to the elongation of groove period. As a result, the droplet on GS with groove width of 8 μm suffers the largest pinning force. So, on different GSs, the pinning force varies. How the surface morphology affects the pinning force? Here, to address this problem, the energy minimization method was adopted.

The work done by pinning force is $\delta W = f \cdot A$, where $A \sim \pi(nD)^2$ is the wetted area of a droplet, and D is the period of groove. When a droplet reaches equilibrium state, the work done by pinning force has the relation of $\mathrm{d}w / \mathrm{d}x = 0$. Namely, $\mathrm{d}(f \cdot A) / \mathrm{d}x = 0$, and the expression can be written as:

$$\frac{\mathrm{d}(fA)}{\mathrm{d}x} = A\frac{\mathrm{d}f}{\mathrm{d}x} + f\frac{\mathrm{d}A}{\mathrm{d}x} = A\frac{\mathrm{d}f}{n\mathrm{d}D} + f\frac{\mathrm{d}A}{n\mathrm{d}D} = 0, \tag{4}$$

and this equation can be simplified as:

$$\frac{\mathrm{d}f}{f} + 2\frac{\mathrm{d}D}{D} = 0, \tag{5}$$

namely,

$$\ln f = -2\ln(\eta D). \tag{6}$$

Then we can get the scaling law between f and D as $f \sim \zeta D^{-2}$, where η and ζ are two constants. When the depth of the groove is fixed, S_c has an inverse relation with D. So, the relation between f and S_c can be expressed as: $f \sim \zeta S_c^2$. The change of CA follows the relation of $\Delta\theta \sim \zeta S_c^2 l / \gamma_{lv}$. Thus, θ_c / θ and S_c have the relationship of:

$$\frac{\theta_c}{\theta} = 1 + \frac{\Delta\theta}{\theta} \sim 1 + \frac{\zeta l}{\theta\gamma_{lv}} S_c^2, \tag{7}$$

where θ_c / θ is a quadratic function of the anisotropic roughness S_c. The scaling law agrees with the experimental results.

3.2 The calculation of CA at any point along the contact line

The relation of CAs in parallel and perpendicular directions was further investigated by the calculation of CA at any point along the elliptical contact line. Here, only the liquids with high surface tension are considered, because of these liquid droplets have apparent ellipsoidal cap shapes. The ellipsoidal cap droplets can be classified into two types: (1) the small ellipsoidal cap model; (2) the large ellipsoidal cap model. The small ellipsoidal cap model corresponds to the droplet whose CAs along elliptic contact line are all smaller than 90°, and large ellipsoidal cap model corresponds to the droplet whose CAs are larger than 90°.

Here, we proposed ellipsoidal cap as the mathematic model for the droplets, as shown in Figure 7(a). Ellipsoidal surface can be expressed with the function of $\frac{x^2}{a^2} + \frac{y^2}{b^2} + \frac{z^2}{c^2} = 1$ ($a > b > c > 0$, and they denote the semi-major axes in X, Y and Z directions, respectively). The cosine value of the angle between tangent plane and X-Y plane at any point (when X-Y plane is taken as droplet bottom, the angle will be CA) can be expressed as:

$$\cos\theta = \frac{2z_0 / c^2}{\sqrt{(2x/a^2)^2 + (2y/b^2)^2 + (2z/c^2)^2}}, \tag{8}$$

where a, b, c and z_0 are four constants once the surface structure is fixed. The calculation of CAs is based on the condition of $z = z_0$, while z_0 represents the bottom level of droplet in z axis, as shown in Figure 7(c). The cosine value of CA can be calculated when the four parameters are given. In experiments, the cosine values of CAs and the semi-major axes of

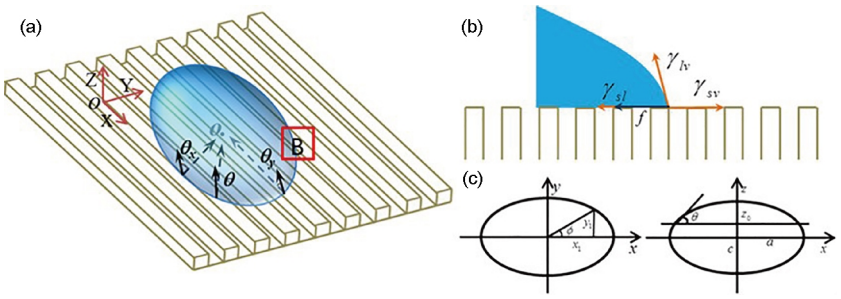

Figure 7 (Color online) Schematic of ellipsoidal cap model. (a) θ_x, θ_y and θ are presented. A mathematic model of ellipsoidal cap is adopted to calculate the arbitrary CA along the elliptic contact line. X, Y and Z directions are defined as shown above. (b) Droplet stays stable under the balance of surface tensions and pinning force on GS. (c) The geometrical model of the cross section and longitudinal section of ellipsoidal cap droplet. a, b, c and z_0 defined in context are presented above. a_1, b_1 are the semi-major axes of elliptic contact line. ϕ is the angle between view direction and groove direction.

a droplet in X and Y directions can be obtained. Then we can get the equations of:

$$\cos\theta_x = \frac{a\sqrt{a^2-a_1^2}}{\sqrt{a^2c^2+\left(a^2-a_1^2\right)\left(b^2-c^2\right)}}, \tag{9}$$

$$\cos\theta_y = \frac{b\sqrt{b^2-a_1^2}}{\sqrt{b^2c^2+\left(b^2-b_1^2\right)\left(a^2-c^2\right)}}, \tag{10}$$

$$a_1^2c^2 = a^2\left(c^2-z_0^2\right), \tag{11}$$

$$b_1^2c^2 = b^2\left(c^2-z_0^2\right), \tag{12}$$

where a_1, b_1 are the semi-major axes of the ellipse while $z = z_0$. For small ellipsoidal cap droplets, z_0 should take positive value. For large ellipsoidal cap droplets, z_0 should take negative value. Combining eqs. (8)–(12), we can determine the four parameters a, b, c and z_0, and then the CA along the contact line can be obtained.

The results of DI water droplet on GS are shown in Figure 8, with S_c being 0.57. And θ_x is 146.8° (Figure 8(a)), θ_y is 123.2° (Figure 8(b)). The droplet image from top view is shown in Figure 8(c). A cross angle ϕ (acute angle) is defined as the angle from groove direction to measure direction of θ. Figure 8(d) shows the experimental data and the theoretical values, and the theoretical values agree with the experimental data well. This result demonstrates that the ellipsoidal model is effective for the calculation of CAs on GS.

3.3 Symbolical contact angle (SCA) for ellipsoidal cap droplet

CA of droplets on GS varies in different position on elliptic contact line. The variation of CA results in many inconveniences in the characterization of anisotropic wetting. Until now, there is still no definition of hydrophobicity of GS due to the non-uniform CAs of droplets on GS, especially for the case that $\theta_x > 90°$ and $\theta_y < 90°$. Thus, a CA to characterize the anisotropic wetting behavior of a droplet on GS is essential to the study of wetting on GS. Our results indicated that the CAs around the contact line vary as a rule of elliptic function, as shown in Figure 9(a). Here, we assume that SCA also has a quadratic relation with θ_x and θ_y. To indicate the contributions of θ_x and θ_y to SCA, we suggested the following equation:

$$\left(\frac{\theta_s}{\theta_x}\right)^2+\left(\frac{\theta_s}{\theta_y}\right)^2 = 2, \tag{13}$$

where θ_s is SCA. From this equation, we defined the SCA as:

$$\theta_s = \sqrt{\frac{2\theta_x^2\theta_y^2}{\theta_x^2+\theta_y^2}}. \tag{14}$$

The cubical relation or other forms of SCA is also available, however, the cubical relation is fluctuating too much compared to the quadratic relation. The form of SCA above is simple yet unique compared to other forms. The above equation would be feasible to address this SCA problem only when four conditions are satisfied: (1) SCA should be able to reflect the properties of droplet and material surface. Moreover, one SCA corresponds to one given surface and liquid. (2) SCA should change with surface properties monotonously, and the relation between SCA and materials surface properties should be regular and easy to obtain. (3) The parameters in the expression are easy to get from experiments. (4) The expression can be degenerated to the equation on homogeneous smooth surface.

θ_x, θ_y and θ_s will be fixed when surface structure and liquid are given, as shown in Figure 9(b). The square of θ_x and θ_y in the expression ensures the uniqueness for the characterization of one given pair of surface and liquid. Furthermore, in experiments, the values of θ_x and θ_y are easy to be obtained. When the droplet is on smooth surface, θ_s equals to θ_x and θ_y. The equation above can be degenerated to that on smooth surface to satisfy the condition (4). From the experiments and the satisfied conditions, the SCA is feasible to characterize the droplet properties on GS.

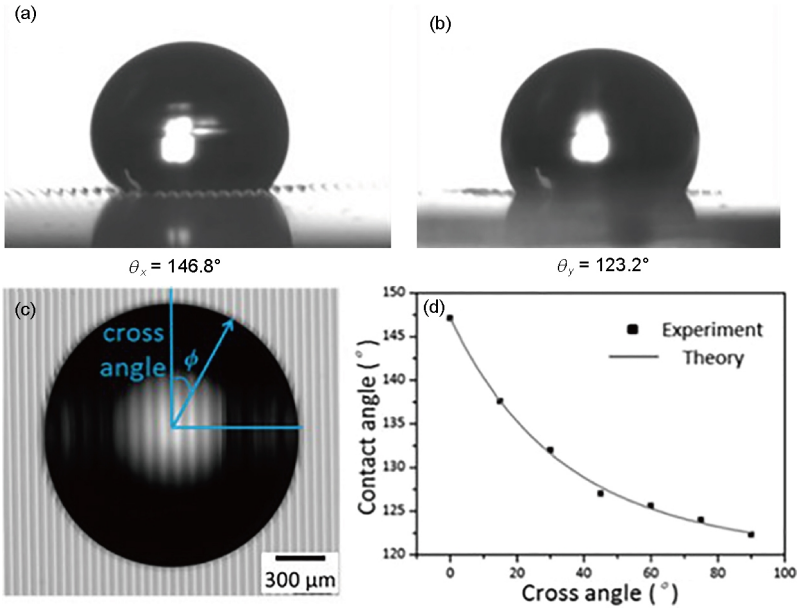

Figure 8 (Color online) The images of a droplet on GS observed from different views. (a) Front view, and θ_x=146.8°; (b) side view, and θ_y=123.2°; (c) top view, with the outline of the droplet being elliptic. The cross angle ϕ is defined as angle from groove direction to view direction. (d) The experimental data and theoretical values of CAs with respect to the cross angle. The theoretical values fit experimental data well.

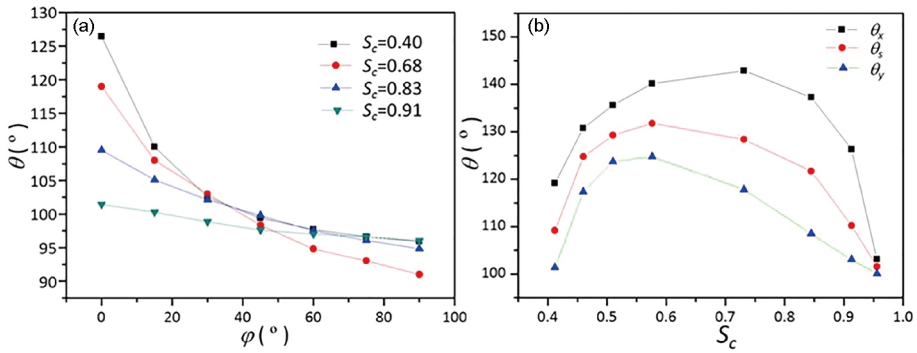

Figure 9 (Color online) The experimental data and the calculated SCA adopting the eq. (13). (a) CAs vary with aspect to cross angle with different S_c. CA varies with a rule of elliptic function curve. (b) For the varied S_c, CA changes by the tendency of increasing first and then decreasing. The calculated SCAs are between the CAs in X and Y directions. When S_c closes to 1, SCA tends to have the values of CAs in X and Y directions.

4 Conclusions

In summary, the anisotropic behavior of a droplet on GS was studied experimentally and theoretically in this paper. The relationship between CA and S_c was analyzed. From the experimental results, we found that CA increases first and then decreases with increasing groove period. The variation of CA shows a nonlinear relation with S_c. The theoretical analysis manifested that in the perpendicular direction the CA is a quadratic function with S_c. A mathematical model was suggested to calculate the CA of an ellipsoid cap droplet. In this simple model, we regarded the droplet on GS as a part of an ellipsoid. The calculated values match experimental data well for droplets of high surface tension. We offered a simple and convenient method to characterize the wettability of a droplet on GS. And this method satisfies the demands that characterizing a droplet on GS. Our results may be helpful to a further understanding of the anisotropic wetting on GS and will assist the potential design in related products in the future.

This work was supported by the National Natural Science Foundation of China (Grant Nos. U1562105, 11611130019 and 11372313), the Chinese Academy of Sciences (CAS) through CAS Interdisciplinary Innovation Team Project, the CAS Key Research Program of Frontier Sciences (Grant No. QYZDJ-SSW-JSC019), and the CAS Strategic Priority Research Program (Grant No. XDB22040401).

1 Zhao Y P. Physical Mechanics of Surfaces and Interfaces (in Chinese). Beijing: Science Press, 2012
2 Sun G, Fang Y, Cong Q, et al. Anisotropism of the non-smooth surface of butterfly wing. J Bionic Eng, 2009, 6: 71–76
3 Vernik L, Liu X. Velocity anisotropy in shales: A petrophysical study. Geophysics, 1997, 62: 521–532
4 Xia D, Johnson L M, López G P. Anisotropic wetting surfaces with one-dimesional and directional structures: Fabrication approaches,

wetting properties and potential applications. Adv Mater, 2012, 24: 1287–1302
5 Yuan Q, Huang X, Zhao Y P. Dynamic spreading on pillar-arrayed surfaces: Viscous resistance versus molecular friction. Phys Fluids, 2014, 26: 092104
6 Quéré D. Wetting and roughness. Annu Rev Mater Res, 2008, 38: 71–99
7 Parker A R, Lawrence C R. Water capture by a desert beetle.. Nature, 2001, 414: 33–34
8 Yuan Q, Zhao Y P. Wetting on flexible hydrophilic pillar-arrays. Sci Rep, 2013, 3: 1944
9 Chen L, Auernhammer G K, Bonaccurso E. Short time wetting dynamics on soft surfaces. Soft Matter, 2011, 7: 9084–9089
10 Kreder M J, Alvarenga J, Kim P, et al. Design of anti-icing surfaces: Smooth, textured or slippery? Nat Rev Mater, 2016, 1: 15003
11 Wang S, Yang Z, Gong G, et al. Icephobicity of penguins *Spheniscus Humboldti* and an artificial replica of penguin feather with air-infused hierarchical rough structures. J Phys Chem C, 2016, 120: 15923–15929
12 Wen C Y, Tersoff J, Hillerich K, et al. Periodically changing morphology of the growth interface in Si, Ge, and GaP nanowires. Phys Rev Lett, 2011, 107: 025503
13 Jacobsson D, Panciera F, Tersoff J, et al. Interface dynamics and crystal phase switching in GaAs nanowires. Nature, 2016, 531: 317–322
14 Schutzius T M, Jung S, Maitra T, et al. Spontaneous droplet trampolining on rigid superhydrophobic surfaces. Nature, 2015, 527: 82–85
15 Dubov A L, Mourran A, Möller M, et al. Contact angle hysteresis on superhydrophobic stripes. J Chem Phys, 2014, 141: 074710
16 Chi L F, Gleiche M, Fuchs H. Nanoscopic channel lattices with controlled anisotropic wetting. Nature, 2000, 403: 173–175
17 Yu N, Wang S, Liu Y, et al. Thermal-responsive anisotropic wetting microstructures for manipulation of fluids in microfluidics. Langmuir, 2017, 33: 494–502
18 Wang Z, Zhao Y P. Wetting and electrowetting on corrugated substrates. Phys Fluids, 2017, 29: 067101
19 Brandon S, Haimovich N, Yeger E, et al. Partial wetting of chemically patterned surfaces: The effect of drop size. J Colloid Interface Sci, 2003, 263: 237–243
20 Fürstner R, Barthlott W, Neinhuis C, et al. Wetting and self-cleaning properties of artificial superhydrophobic surfaces. Langmuir, 2005, 21: 956–961
21 Liu C, Ju J, Ma J, et al. Directional drop transport achieved on high-temperature anisotropic wetting surfaces. Adv Mater, 2014, 26: 6086–6091
22 Seemann R, Brinkmann M, Kramer E J, et al. Wetting morphologies at microstructured surfaces. Proc Natl Acad Sci USA, 2005, 102: 1848–1852
23 Chu K H, Xiao R, Wang E N. Uni-directional liquid spreading on asymmetric nanostructured surfaces. Nat Mater, 2010, 9: 413–417
24 Park K C, Kim P, Grinthal A, et al. Condensation on slippery asymmetric bumps. Nature, 2016, 531: 78–82
25 Xia D, Brueck S R J. Strongly anisotropic wetting on one-dimensional nanopatterned surfaces. Nano Lett, 2008, 8: 2819–2824
26 Wenzel R N. Resistance of solid surfaces to wetting by water. Ind Eng Chem, 1936, 28: 988–994
27 Cassie A B D, Baxter S. Wettability of porous surfaces. Trans Faraday Soc, 1944, 40: 546–551
28 Yang J, Rose F R A J, Gadegaard N, et al. Effect of sessile drop volume on the wetting anisotropy observed on grooved surfaces. Langmuir, 2009, 25: 2567–2571
29 Hirvi J T, Pakkanen T A. Wetting of nanogrooved polymer surfaces. Langmuir, 2007, 23: 7724–7729
30 Zhao Y, Lu Q, Li M, et al. Anisotropic wetting characteristics on submicrometer-scale periodic grooved surface. Langmuir, 2007, 23: 6212–6217
31 Li W, Fang G, Li Y, et al. Anisotropic wetting behavior arising from superhydrophobic surfaces: Parallel grooved structure. J Phys Chem B, 2008, 112: 7234–7243
32 Chen Y, He B, Lee J, et al. Anisotropy in the wetting of rough surfaces. J Colloid Interface Sci, 2005, 281: 458–464
33 Kusumaatmaja H, Vrancken R J, Bastiaansen C W M, et al. Anisotropic drop morphologies on corrugated surfaces. Langmuir, 2008, 24: 7299–7308
34 Chung J Y, Youngblood J P, Stafford C M. Anisotropic wetting on tunable micro-wrinkled surfaces. Soft Matter, 2007, 3: 1163–1169
35 Zhao Y P. Bridging length and time scales in moving contact line problems. Sci China-Phys Mech Astron, 2016, 59: 114631
36 Yuan Q, Zhao Y P. Topology-dominated dynamic wetting of the precursor chain in a hydrophilic interior corner. Proc R Soc A-Math Phys Eng Sci, 2012, 468: 310–322
37 Bell M S, Shahraz A, Fichthorn K A, et al. Effects of hierarchical surface roughness on droplet contact angle. Langmuir, 2015, 31: 6752–6762
38 Feng L, Li S, Li Y, et al. Super-hydrophobic surfaces: From natural to artificial. Adv Mater, 2002, 14: 1857–1860
39 De Gennes P G, Brochard-Wyart F, Quéré D. Capillarity and Wetting Phenomena: Drops, Bubbles, Pearls, Waves. New York: Springer, 2004
40 Zhao Y P. Nano and Mesoscopic Mechanics (in Chinese). Beijing: Science Press, 2014
41 Sefiane K. Effect of nonionic surfactant on wetting behavior of an evaporating drop under a reduced pressure environment. J Colloid Interface Sci, 2004, 272: 411–419